



PERGAMON

Journal of the Mechanics and Physics of Solids  
50 (2002) 681–694

---

---

JOURNAL OF THE  
MECHANICS AND  
PHYSICS OF SOLIDS

---

---

www.elsevier.com/locate/jmps

# The correlation of the indentation size effect measured with indenters of various shapes

J.G. Swadener<sup>a,b,\*</sup>, E.P. George<sup>a</sup>, G.M. Pharr<sup>a,b</sup>

<sup>a</sup>*Metals and Ceramics Division, Oak Ridge National Laboratory, P.O. Box 2008, Oak Ridge, TN 37831, USA*

<sup>b</sup>*Department of Materials Science and Engineering, University of Tennessee, Knoxville, TN 37996, USA*

Received 26 April 2001; received in revised form 6 July 2001

---

## Abstract

◇ Experimental results are presented which show that the indentation size effect for pyramidal and spherical indenters can be correlated. For a pyramidal indenter, the hardness measured in crystalline materials usually increases with decreasing depth of penetration, which is known as the indentation size effect. Spherical indentation also shows an indentation size effect. However, for a spherical indenter, hardness is not affected by depth, but increases with decreasing sphere radius. The correlation for pyramidal and spherical indenter shapes is based on geometrically necessary dislocations and work-hardening. The Nix and Gao indentation size effect model (J. Mech. Phys. Solids 46 (1998) 411) for conical indenters is extended to indenters of various shapes and compared to the experimental results. © 2002 Elsevier Science Ltd. All rights reserved.

*Keywords:* A. Dislocations; Strengthening and mechanisms; C. Mechanical testing; Indentation and hardness

---

## 1. Introduction

An increase in hardness with decreasing depth of penetration, known as the indentation size effect, has been observed in numerous microindentation studies. Much of the early work was reviewed by Mott (1956). Recent studies (Stelmashenko et al., 1993; De Guzman et al., 1993; Ma and Clark, 1995) have shown a greater increase in hardness for depths less than 1  $\mu\text{m}$ . The related phenomenon of increased yield strength

---

\* Corresponding author. Present address: Los Alamos National Laboratory, MS-G755, P.O. Box 1663, Los Alamos, NM 87545, USA. Fax: +1-865-665-3935.

*E-mail address:* swadener@lanl.gov (J.G. Swadener).

with decreasing specimen size has been observed in microtorsion and microbend experiments (Fleck et al., 1994; Stölken and Evans, 1998). By introducing material length scales into a phenomenological model, Fleck and Hutchinson (1993, 1997) developed a strain gradient plasticity model that describes the behavior. For judicious choices of two length scale parameters, their model matches the microindentation and microtorsion experimental results.

Ashby (1970) proposed that geometrically necessary dislocations (Nye, 1953) would lead to increased strength in bending and in indentation with a flat punch. By considering the geometrically necessary dislocations generated by a conical indenter, Nix and Gao (1998) developed a mechanism-based model that agrees with microindentation results. Their model has undergone further development (Gao et al., 1999a, b; Huang et al., 2000) and has successfully modeled microindentation (Stelmashenko et al., 1993; McElhaney et al., 1998), microtorsion (Fleck et al., 1994) and microbend (Stölken and Evans, 1998) experiments. However, recent microindentation results that cover a greater range of depths show only partial (Poole et al., 1996) or no agreement (Lim and Chaudhri, 1999) with the Nix and Gao model. The indentation results reported herein are also not well described by the Nix and Gao model.

Recently, a method was developed to determine the indentation size effect using spherical indenters (Swadener et al., 2001). Spherical indenters show a dependence of hardness on the radius of the indenter rather than on the depth of penetration (Swadener et al., 2001). Here, the Nix and Gao model is expanded to encompass a wide variety of indenter shapes. The expanded model agrees with recent experimental results for spherical and pyramidal indenter shapes for relatively large spheres and at relatively large depths, respectively, but limitations for small spheres and at small depths are identified.

By taking into account the effects of work hardening, we find a correlation for various indenter shapes, which is based on geometrically necessary dislocations. For spherical and pyramidal indenter shapes, the correlation is corroborated by experiments on iridium reported herein and by previous experiments on oxygen free copper (Lim et al., 1998, 1999)

## 2. Theory

The hypothesis that geometrically necessary dislocations are generated during indentation leads to a method to correlate the indentation size effect for different indenter shapes. Our derivation utilizes the basic precepts given by Nix and Gao (1998) for a conical indenter. By way of introduction, a summary of the Nix and Gao model is given first, followed by the development of a more general theory.

The Nix and Gao (1998) model assumes that plastic deformation of the surface is accompanied by the generation of dislocation loops below the surface, which are contained in an approximately hemispherical volume below the region in contact, as shown schematically in Fig. 1a. Since the indenter is conical, the deformation is self-similar and the angle of the indented surface ( $\theta$ ) remains constant, such that  $\tan \theta = h_p/a$ , where  $h_p$  is the residual plastic depth, and  $a$  is the contact radius. The number of geometri-

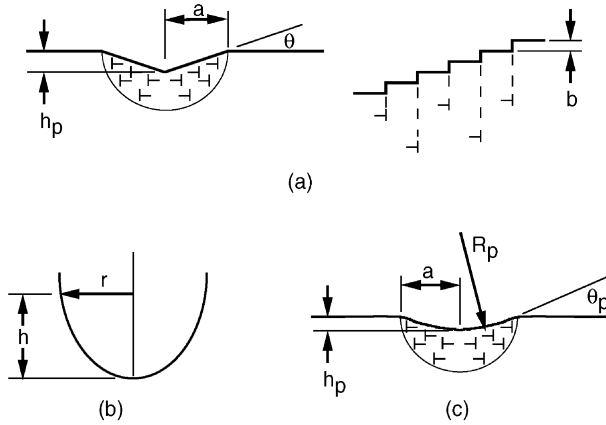


Fig. 1. Model of (a) geometrically necessary dislocations for a conical indent (after Nix and Gao, 1998), (b) a general indenter profile and (c) a spherical indent.

cally necessary dislocation loops is  $h_p/b$ , where  $b$  is Burger’s vector. Integrating from 0 to  $a$  gives the total length of dislocation loops is:  $\lambda = \pi h_p a/b$ . The model assumes that the dislocations are distributed approximately uniformly in a hemispherical volume that scales with the contact radius  $V = 2\pi a^3/3$ . Therefore, the density of the geometrically necessary dislocations is

$$\rho_G = \frac{\lambda}{V} = \frac{3}{2bh_p} \tan^2 \theta. \tag{1}$$

The dislocation density is assumed to be related to the shear strength by the Taylor (1938) hardening model:

$$\tau = \alpha \mu b \sqrt{\rho_T}, \tag{2}$$

where  $\tau$  is the shear strength,  $\mu$  is the shear modulus, and  $\rho_T$  is the total dislocation density. The geometric constant  $\alpha$  in Eq. (2) is usually in the range 0.3–0.6 for FCC metals (Wiedersich, 1964). Arsenlis and Parks (1999) have shown that, due to crystallographic requirements, the actual number of dislocations that must be generated to accommodate plastic deformation is greater than the number of geometrically necessary dislocations by a factor  $\bar{r}$  (called the Nye factor). Therefore, the total dislocation density is  $\rho_T = \bar{r}\rho_G + \rho_S$ , where  $\rho_S$  is the statistically stored dislocation density.

Assuming that the flow stress is related to the shear strength by the Mises flow rule  $\sigma = \sqrt{3}\tau$ , and the hardness is related to flow stress by the Tabor (1951) factor of 3:  $H = 3\sigma$ , the model gives the following expression for the increase in hardness as a function of depth:

$$H = H_0 \sqrt{1 + \frac{h^*}{h_p}}, \tag{3}$$

where  $H_0 = 3\sqrt{3}\alpha\mu b\sqrt{\rho_S}$  and  $h^* = 3\bar{r}\tan^2\theta/2b\rho_S$ .  $H_0$  is the macroscopic hardness, and  $h^*$  is a length scale for the depth dependence of hardness.

The Nix and Gao model can be simply extended to the case of an indenter with a smooth axisymmetric profile of the form  $h = Ar^n$  for  $n > 1$ , where  $A$  is a constant (see Fig. 1b). Following Nix and Gao (1998), the total length of the geometrically necessary dislocation loops ( $\lambda$ ) is found by integrating the number of steps on the indented surface (see Fig. 1):

$$\lambda = \int_0^a \frac{2\pi r}{b} \left( \frac{dh}{dr} \right) dr = \frac{2\pi n A}{b(n+1)} a^{n+1}, \quad (4)$$

where  $a$  is the radius of contact. Assuming, as before, that the geometrically necessary dislocations are contained within a volume  $V = 2\pi a^3/3$ , the average geometrically necessary dislocation density is

$$\rho_G = \frac{\lambda}{V} = \frac{3nA}{b(n+1)} a^{n-2} = \frac{3nA^{(2/n)}}{b(n+1)} h^{(1-2/n)}. \quad (5)$$

In the limit as  $n \rightarrow 1$ ,  $\rho_G$  is proportional to  $h^{-1}$ , and the Nix and Gao model is recovered. For  $1 < n < 2$ , the hardness is predicted to increase with decreasing depth, but the rate of increase would diminish as  $n$  increases from 1 to 2. For the special case of a parabolic indenter ( $n=2$ ), which approximates a spherical indenter at small depths,  $\rho_G$  is not a function of  $h$ , and therefore, the hardness is not dependent on depth. For an indenter geometry with  $n > 2$ , the hardness is expected to decrease with decreasing depth due to the predicted decrease in dislocation density. This last case points out that, contrary to current thought, smaller is not necessarily stronger. The observed increases in strength in microindentation, microtorsion and microbending can all be explained by the geometric dislocation density (Gao et al., 1999a) that results from the geometry of the deformation rather than the specimen size per se.

The shapes of almost all available indenters approximate (to first order) either  $n=1$  (e.g. conical and pyramidal indenters),  $n=2$  (e.g. spheres) or  $n=\infty$  (flat punches). The hardness measured by a flat punch can vary depending on the smoothness of the punch and the rounding of the edges, which makes it unsuitable for this study. The correlation between the other two major classes of indenter geometry will be studied in detail. For a spherical (parabolic) indenter, there is no depth dependence, but there is a dependence of hardness on the radius of the indenter (Swadener et al., 2001).

The profile of a residual impression resulting from spherical indentation is approximately  $h = r^2/2R_p$  (for  $a \ll R_p$ ), where  $R_p$  is the spherical radius of the residual surface impression. Note that  $R_p$  is generally found experimentally to be 10–25% greater than the indenter radius due to partial elastic recovery during unloading. From Eq. (4), the total length of dislocation loops for spherical indentation is  $\lambda = 2\pi a^3/3bR_p$ . The average density of the geometrically necessary dislocations is given by Eq. (5) as

$$\rho_G = \frac{1}{bR_p}. \quad (6)$$

By introducing the material length scale  $R^* = \bar{r}/b\rho_S$  for spherical indentation, we can derive an expression for hardness as a function of  $R_p$  that has the same form as Eq. (3) (Swadener et al., 2001):

$$H = H_0 \sqrt{1 + \frac{R^*}{R_p}}, \quad (7)$$

where  $H_0$  is defined the same as before. Therefore, for spherical indentation, the radius of the impression rather than the depth of penetration determines the indentation size effect. One advantage of the spherical formulation over the conical formulation is that  $R^*$  is written strictly in terms of material constants, whereas the conical formulation includes the geometric term  $\tan \theta$ . The length scales used for other indenter shapes will have a similar geometric term arising from the constant  $A$ . This constant can be eliminated only for spherical or parabolic indenters, because they have no depth dependence.

### 3. Experimental procedure and data analysis

Ultra low-load indentation (nanoindentation) was conducted on a 0.5 mm thick specimen of iridium alloyed with 0.3 pct W and 60 ppm Th. This alloy has good resistance to oxidation and is used in applications requiring high strength and moderate ductility at high temperatures. The addition of W to iridium improves its formability, while Th increases its ductility (Liu et al., 1981; George and Liu, 2000). The specimen was recrystallized for 1 h at 1300°C, which resulted in a grain size of approximately 30  $\mu\text{m}$ . One surface was polished with successively finer media, finishing with 1  $\mu\text{m}$  diamond paste and afterward strain relieved for 1 h at 900°C. Finally, a portion of the polished surface was electropolished to remove surface material affected by mechanical polishing. Atomic force microscopy measurements showed that electropolishing removed approximately 2  $\mu\text{m}$  of the surface. However, no statistically significant differences were found between the indentation results for electropolished and mechanical polished surfaces (Swadener et al., 2001).

Nanoindentation experiments were conducted at 23°C using spherical and Berkovich (three sided pyramid) indenters. Displacements and loads were measured with a resolution of 0.16 nm and 0.3  $\mu\text{N}$ , respectively. For nanoindentation with a diamond Berkovich tip, the continuous stiffness measurement mode was used, and the tip shape was calibrated by conducting experiments on a fused quartz standard (Oliver and Pharr, 1992). Data were analyzed using the Oliver and Pharr (1992) method. Additional hardness tests were conducted using a Berkovich tip at loads of 25–1000 g in a micro-hardness tester and at a load of 15 kg in a Rockwell hardness tester. The loads were calibrated within 0.1%, and the indent areas were measured with a video microscope system, which had a 0.25  $\mu\text{m}$  resolution.

In order to explore a wide variation in spherical radius, five spherical tips were used: a diamond tip with a 14  $\mu\text{m}$  radius of curvature, three sapphire tips with 69, 122 and

318  $\mu\text{m}$  radii, and a 1600  $\mu\text{m}$  radius steel ball. The radii of the diamond and sapphire spherical tips were calibrated from experiments conducted on fused quartz and *c*-axis sapphire (Swadener and Pharr, 2000). The contact radius ( $a$ ) was determined using the geometry of the sphere ( $a^2 = 2Rh_c - h_c^2$ , where  $h_c$  is the contact depth) and the formula developed by Field and Swain (1993):  $h_c = (h_{\text{max}} + h_p)/2$ , where  $h_{\text{max}}$  is the maximum depth and  $h_p$  is the residual depth of the impression after unloading. The quantities  $h_{\text{max}}$  and  $h_p$  are directly measurable. The final radius of curvature of the indent ( $R_p$ , see Fig. 1b) was determined from

$$a^2 = 2R_p h_p - h_p^2. \quad (8)$$

Indentations were made with the 1600  $\mu\text{m}$  steel ball using a Rockwell hardness tester at loads of 15, 30 and 45 N. For these indentations, the contact radius was measured optically.

Uniaxial tensile tests were conducted on iridium specimens in the same recrystallized condition as the indentation specimens. The flow stress was determined from load cell measurements and the specimen dimensions, and the elongation of the gage length was measured using an optical stage at selected increments.

#### 4. Berkovich indenter results

Hardness values obtained with a Berkovich indenter were determined from the continuous stiffness measurements using the Oliver and Pharr method for data ranging from depths of 30 nm to 1.8  $\mu\text{m}$  and for maximum loads up to 300 mN. Following the method proposed by Nix and Gao (1998), the hardness results obtained from nanoindentation, microindentation and a Rockwell hardness tester fitted with a Berkovich tip are plotted in Fig. 2 as  $(H/H_0)^2$  versus  $1/h_p$ . A value of  $H_0 = 2.5$  GPa, corresponding to the measured hardness at the greatest depth tested (50  $\mu\text{m}$ ), was used for this plot. Over the range where microhardness and nanohardness results overlap, there is close agreement. At depths less than 50 nm, rounding of the indenter tip influences the hardness measurement. Therefore, we restrict our discussion to depths greater than 50 nm. The Nix and Gao model prediction for  $H_0 = 2.5$  GPa and  $h^* = 2.6$   $\mu\text{m}$  is also shown in Fig. 2 for comparison. The prediction agrees with the microhardness data within one standard deviation, but diverges significantly from the nanohardness results for  $h_p < 1$   $\mu\text{m}$ .

Although the chosen parameters of  $H_0 = 2.5$  GPa and  $h^* = 2.6$   $\mu\text{m}$  provide accurate agreement of the model with the microhardness results, it will be shown that these values do not agree with spherical indentation results. Even at a depth of 50  $\mu\text{m}$ , the measured hardness is still decreasing with increasing depth and has not yet reached a plateau value corresponding to a macroscopic hardness ( $H_0$ ). Therefore, the value of  $H_0$  is somewhat overestimated. Using a smaller value of  $H_0$  in the model prediction would result in less accurate agreement with the experimental results. The continuing variation

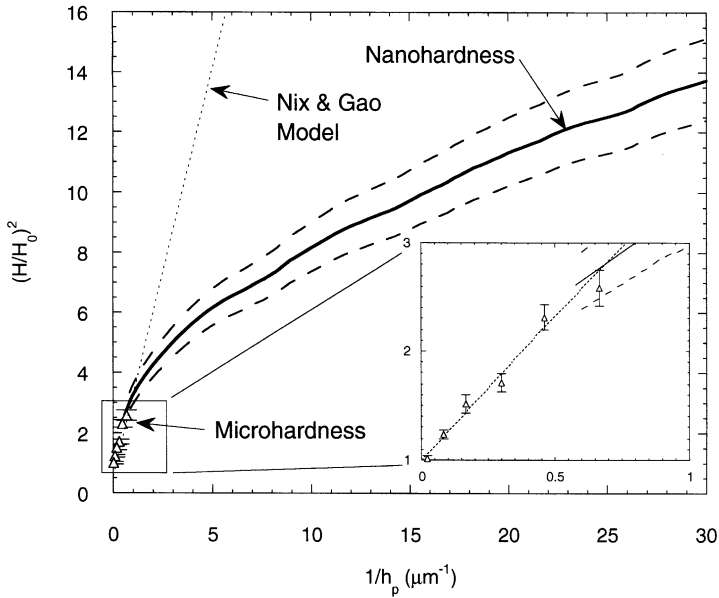


Fig. 2. Indentation size effect in annealed iridium measured with a Berkovich indenter ( $\Delta$  and solid line) and comparison of experiments with the Nix and Gao (1998) model for  $H_0 = 2.5$  GPa and  $h_p = 2.6 \mu\text{m}$  (dotted line). The dashed lines represent + and – one standard deviation of the nanohardness data.

of the measured hardness reported here at relatively large depths is qualitatively similar to the Vickers hardness results of Schultz and Hanemann (1941) for single crystal aluminum and the results of Lim and Chaudhri (1999) for annealed oxygen free copper.

### 5. Spherical indenter results

The hardness for the five spherical indenters used in this study is plotted versus  $a/R$  in Fig. 3. For a spherical indenter, Johnson (1970) has shown that indentation data can be compared with tensile data by utilizing an effective strain of  $0.2a/R$ , which is indicated on the upper ordinate in Fig. 3. For  $a/R < 0.03$ , the hardness increases rapidly due to the transition from elastic dominated to plastic dominated deformation (Johnson, 1970). For  $a/R > 0.03$ , the hardness measured by each sphere increases at a rate approximately parallel to three times the flow stress ( $s_f$ ) plotted versus effective strain as shown in Fig. 3. The flow stress was determined from uniaxial tension tests, in which the material exhibited linear work hardening. The contact radii were determined from the measured depths, and, for several indents, the accuracy was checked using optical and atomic force microscopy (AFM). For the 14, 69 and 122  $\mu\text{m}$  spheres, the contact radius measurements were within  $\pm 7\%$  for all three methods. For the 318  $\mu\text{m}$  radius sphere, optical and AFM measurements of the contact radius were consistently 10–20% smaller than those given by depth measurements. For plotting purposes, the mean

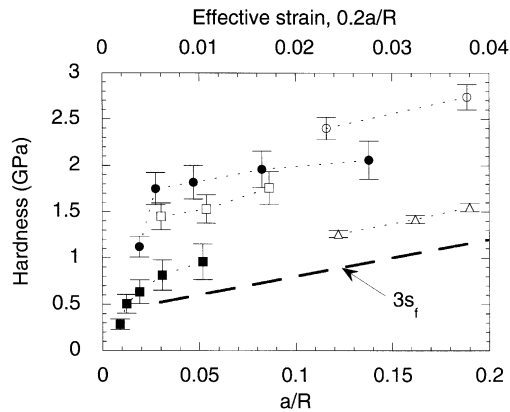


Fig. 3. Variation of hardness in annealed iridium with  $a/R$  for spherical indenters: comparison of experiments ( $R = 14 \mu\text{m}$  ( $\circ$ );  $R = 69 \mu\text{m}$  ( $\bullet$ );  $R = 122 \mu\text{m}$  ( $\square$ );  $R = 318 \mu\text{m}$  ( $\blacksquare$ );  $R = 1600 \mu\text{m}$  ( $\triangle$ )) and the Tabor relation for tensile flow stress ( $3s_f$ ).

values from the three measurement methods were used with error bars representing one standard deviation of all the measurements. The contact radius of the  $1600 \mu\text{m}$  sphere was measured only by optical methods.

The data shown in Fig. 3 points out the chief advantage of using spherical indentation: since the size effect for a spherical indenter is not related to the depth of penetration, the effects of work hardening can be de-coupled from the indentation size effect. Work hardening effects are seen for each sphere as the linear increase in hardness with increasing  $a/R$ , while the different hardness values for different spheres at the same value of  $a/R$  illustrate the indentation size effect. The data also shows that the differences in hardness for the different spheres are not the result of a surface effect or a surface layer, which have been suggested as alternative explanations for the indentation size effect (Shi and Atkinson, 1990; Shaw et al., 1996; Liu and Ngan, 2001). For the same contact radius ( $a$ ), the same amount of surface is in contact, yet the differences in hardness for the same value of  $a$  are even greater than for the same value of  $a/R$ . Therefore, the increase in hardness for the smaller three spheres shown in Fig. 3 cannot be due to a surface effect, such as friction. Also for the same contact radius, a smaller sphere penetrates to a greater depth than a larger sphere. Therefore, the large increase in hardness for the smaller spheres cannot be due to a hardened surface layer.

Because of the effects of work hardening, comparison of the hardness results for the different spheres must be done at the same effective strain and thus the same  $a/R$  value, which requires extrapolation of some of the data. The data for the  $14 \mu\text{m}$  and  $1600 \mu\text{m}$  spherical tips were extrapolated parallel to the tensile work hardening curve to  $a/R = 0.05$ , which is within the fully plastic regime but where the effects of work hardening are small. The hardness for  $a/R = 0.05$  (1% effective strain) for the five spherical tips is shown in Fig. 4. For the  $1600 \mu\text{m}$  sphere,  $R_p$  was estimated to be  $1.1R$ . For the other spheres,  $R_p$  was determined from Eq. (8). The average hardness is approximately the same for the largest two spheres, but increases monotonically

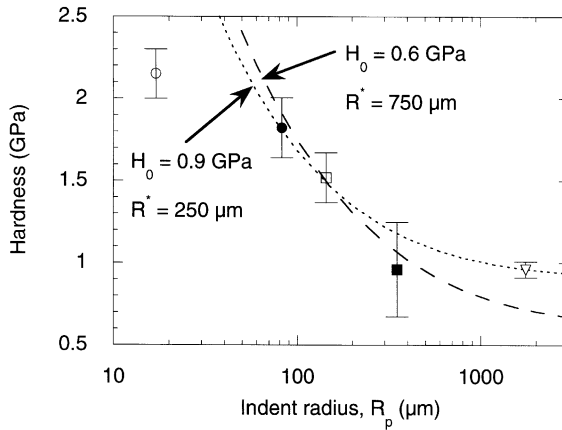


Fig. 4. Indentation size effect in annealed iridium measured with spherical indenters: comparison of experiments in iridium  $a/R=0.05$  ( $R=14\ \mu\text{m}$  ( $\circ$ );  $R=69\ \mu\text{m}$  ( $\bullet$ );  $R=122\ \mu\text{m}$  ( $\square$ );  $R=318\ \mu\text{m}$  ( $\blacksquare$ );  $R=1600\ \mu\text{m}$  ( $\triangle$ )) with the general model for two sets of parameters (dotted line and dashed line).

cally with decreasing  $R_p$  for the other indenters. Hardness values, which were determined from Eq. (7) using two different sets of material parameters, are shown also in Fig. 4. The parameters  $H_0=0.9\ \text{GPa}$  and  $R^*=250\ \mu\text{m}$  provide a good fit to the data for large spheres, but the Tabor relation suggests that  $H_0$  should be  $0.6\ \text{GPa}$ , which is three times the flow stress at 1% strain. For  $H_0=0.9\ \text{GPa}$ ,  $R^*=250\ \mu\text{m}$  and  $\bar{r}=2$ , the value of  $\alpha$  is determined from the definition of  $H_0$  and  $R^*$  as  $0.52$ , while for  $H_0=0.6\ \text{GPa}$ ,  $R^*=750\ \mu\text{m}$  and  $\bar{r}=2$ ,  $\alpha=0.60$ , both of which are within the range expected for  $\alpha$  (Wiedersich, 1964). For either of these choices of parameters, the hardness predicted by Eq. (5) agrees reasonably well with the experimental results for  $R_p > 80\ \mu\text{m}$ , but diverges for smaller values of  $R_p$ . Spherical indentation studies are often conducted with spherical radii as small as  $1\ \mu\text{m}$ , but length scale effects are often overlooked. These results point out that length scale effects must be considered when interpreting indentation results obtained with small spheres.

## 6. Correlation of results

Work hardening also affects the Berkovich hardness results, but in a different manner. Johnson (1970) has shown that the hardness measured by a Berkovich or a Vickers indenter corresponds to an effective strain of 7%, while the hardness values determined by spherical indenters are evaluated at an effective strain of 1%. Based on the observed work-hardening in tensile test results, the expected difference between hardness values determined at 1% and 7% effective strain values is  $1.2\ \text{GPa}$ . Decreasing the hardness determined by a Berkovich indenter in Fig. 2 by  $1.2\ \text{GPa}$  brings these values at large depths into the range of the spherical data in Fig. 4.

A correlation of the indentation size effect determined with the two indenter geometries (spherical and pyramidal) can be determined from the geometrically necessary

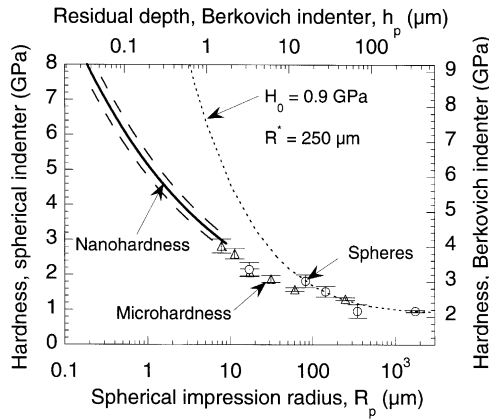


Fig. 5. Correlation of the indentation size effect in annealed iridium measured with spherical indenters at  $a/R=0.05$  (○), with a Berkovich indenter (Δ and solid line) and comparison of experiments with the general model (dotted line).

dislocations required by each indenter. The total length of geometrically necessary dislocation loops required by a spherical indenter is  $\lambda = 2.09a^3/bR_p$  and a Berkovich or Vickers indenter ( $\tan \theta = 0.358$ ) requires a total length of  $\lambda = 0.403a^3/bh_p$ . Therefore, for  $R_p = 5.2h_p$ , the same total length of geometrically necessary dislocation loops is required, and the hardness measured by the two indenters is expected to be the same. By definition, the same ratio ( $R^* = 5.2h^*$ ) holds for the relation between the length scales used in the modeling of the indentation size effect by spherical and conical indenters with  $\tan \theta = 0.358$ . Fig. 5 shows this correlation by using the  $R_p = 5.2h_p$  relation and plotting the hardness measured by a Berkovich indenter offset by 1.2 GPa to account for work hardening. The results for the two indenter shapes agree within one standard deviation, which corroborates the proposed correlation.

The above correlation procedure was also applied to the results obtained by Lim et al. (1998, 1999) for spherical and pyramidal indentation of oxygen free copper (OFC). The value of  $R_p$  was not reported, but is assumed to be  $1.1R$ . From compression tests of annealed OFC (Lim and Chaudhri, 1999), work hardening is predicted to result in an increase in hardness of 0.24 GPa for a Berkovich or Vickers indenter compared to the hardness measured by a spherical indenter at  $a/R=0.05$ . The hardness results from Lim et al. are plotted in Fig. 6 with the results for pyramidal indenters offset by 0.24 GPa. The proposed correlation brings the spherical and pyramidal indenter results into agreement with perhaps the exception of the smallest ( $R=7 \mu\text{m}$ ) sphere.

Using  $H_0 = 0.12 \text{ GPa}$  and  $R^* = 200 \mu\text{m}$ , Fig. 6 shows that the hardness predicted by Eq. (7) agrees with the experimental results for  $R_p > 8 \mu\text{m}$  ( $h_p > 1.5 \mu\text{m}$ ). For  $R_p < 8 \mu\text{m}$ , the model overestimates the hardness in the same manner as for iridium. For  $H_0 = 0.12 \text{ GPa}$  and  $R^* = 200 \mu\text{m}$ ,  $\alpha = 0.33$ , which agrees with previous results for copper (Wiedersich, 1964). Thus, the disagreement of the Nix and Gao model with experimental results for pyramidal indentation in annealed OFC (Lim and Chaudhri, 1999) can be largely corrected by compensating for work hardening during indentation.

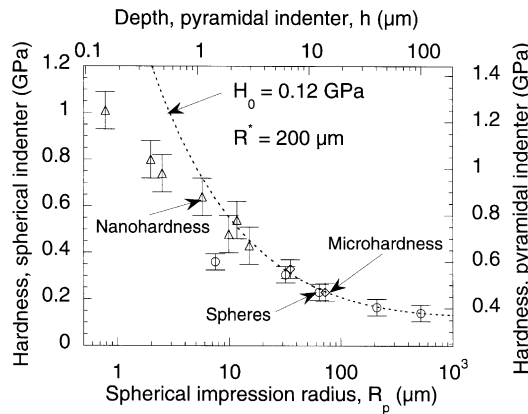


Fig. 6. Correlation of the indentation size effect in annealed oxygen-free copper measured with spherical indenters at  $a/R = 0.05$  ( $\circ$ ), with a Berkovich indenter ( $\triangle$ ) and with a Vickers indenter ( $\diamond$ ) (data from Lim et al., 1998, 1999) and comparison of experiments with the general model (dotted line).

The indentation results indicate that the macroscopic hardness is 0.12 GPa, although the Tabor relation predicts  $H_0 = 0.18$  GPa. Note that the Tabor relation overestimates the macroscopic hardness of annealed OFC, while it underestimates the apparent macroscopic hardness of iridium.

Lim et al. (1998, 1999) also conducted indentation on OFC that they cold-worked to a strain of approximately 0.6. For OFC with this degree of cold-work, very little additional work hardening occurs during indentation. Therefore, for this material, the hardness measured by spherical and pyramidal indenters is not expected to be offset by work hardening. For cold-worked OFC, the macroscopic hardness was determined to be 0.9 GPa (Lim and Chaudhri, 1999). Using  $H_0 = 0.9$  GPa and  $\alpha = 0.33$   $\mu\text{m}$ , as determined above for OFC, implies that  $R^* = 3.6$   $\mu\text{m}$ . Predictions from Eq. (7) using  $H_0 = 0.9$  GPa and  $R^* = 3.6$   $\mu\text{m}$  are compared to experimental results for cold-worked OFC in Fig. 7. The results for spherical and pyramidal indenters are correlated using the theory developed above. Although the model overestimates the hardness at small values of  $R_p$  and  $h_p$ , it fits the data well for  $R_p > 5$   $\mu\text{m}$  ( $h_p > 1$   $\mu\text{m}$ ). Since the predictions for annealed OFC deviate from the experimental results at  $H = 0.6$  GPa, the deviation of the predictions for cold-worked OFC from the experimental results at  $H = 1.1$  GPa are not surprising.

## 7. Discussion

Since, as shown in Figs. 5–7, predictions from Eq. (7) overestimate hardness for small values of  $h_p$  or  $R_p$ , some discussion of the cause for this discrepancy is warranted. The form of the Taylor hardening model has been found to be reasonably accurate for FCC metals such as aluminum (Taylor, 1938) and copper (Wiedersich, 1964). The correlation of the indentation size effect for the two different indenter shapes suggests that the expressions used for the total dislocation line length  $\lambda$  are reasonably accurate,

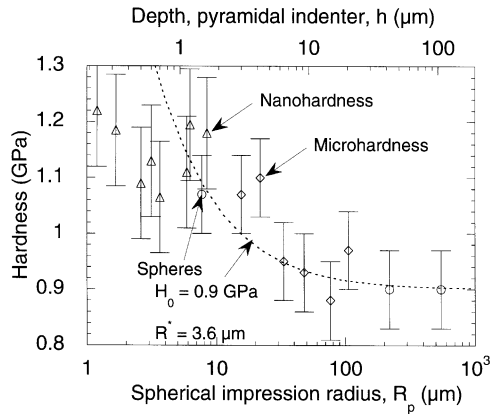


Fig. 7. Correlation of the indentation size effect in cold-worked oxygen-free copper measured with spherical indenters at  $a/R = 0.05$  ( $\circ$ ), with a Berkovich indenter ( $\triangle$ ) and with a Vickers indenter ( $\diamond$ ) (data from Lim et al., 1998, 1999) and comparison of experiments with the general model (dotted line).

even in regions where the model overestimates the hardness. Therefore, the most likely source of error in the model is the assumption that the dislocations are confined within a hemispherical volume that scales with the contact radius. For the larger dislocation densities that are predicted for smaller values of  $h_p$  and  $R_p$ , repulsive forces between dislocations may cause the dislocations to spread beyond the assumed hemispherical volume. Dislocation repulsion would cause the measured hardness to be less than the model prediction and could give rise to the experimental results shown in Fig. 6. Additional studies are required to develop a more complete model.

## 8. Conclusions

A method for determining the indentation size effect for a general indenter geometry has been developed. The spherical indenter was shown to be a special case that does not show depth dependence in hardness, but does show a dependence on the radius of the sphere. This dependence on the indenter radius rather than on depth offers both practical advantages and provides the basis for a more comprehensive method of analyzing material length scales. With the new method, the effects of work hardening and the material length scale can be uncoupled and determined independently. The correlation of the indentation size effect measured by spherical and pyramidal indenters was demonstrated in iridium and oxygen free copper. The correlation of results from spherical and pyramidal shapes indicates that the simple model for the number of geometrically necessary dislocations is sufficiently accurate. However, the model predictions deviate from the experimental results at small radii for the case of spherical indenters and at small depths in the case of pyramidal indenters. This deviation indicates that the volume occupied by the geometrically necessary dislocations at high dislocation densities is probably inaccurate and requires further study.

## Acknowledgements

Research at the Oak Ridge National Laboratory SHaRE User Facility was sponsored by the Office of Space and Power Systems and by the Division of Materials Sciences and Engineering, U.S. Department of Energy, under contract DE-AC05-00OR22725 with UT-Battelle, LLC.

## References

- Arsenlis, A., Parks, D.M., 1999. Crystallographic aspects of geometrically-necessary and statistically-stored dislocation density. *Acta Mater.* 47, 1597–1611.
- Ashby, M.F., 1970. The deformation of plastically non-homogenous materials. *Philos. Mag.* 21, 399–424.
- De Guzman, M.S., Neubauer, G., Flinn, P., Nix, W.D., 1993. The role of indentation depth on the measured hardness of materials. *Mater. Res. Soc. Symp. Proc.* 308, 613–618.
- Field, J.S., Swain, M.V., 1993. A simple predictive model for spherical indentation. *J. Mater. Res.* 8, 297–306.
- Fleck, N.A., Hutchinson, J.W., 1993. A phenomenological theory for strain gradient effects in plasticity. *J. Mech. Phys. Solids* 41, 1825–1857.
- Fleck, N.A., Hutchinson, J.W., 1997. Strain gradient plasticity. In: Hutchinson, J.W., Wu, T.Y. (Eds.), *Advances in Applied Mechanics*, Vol. 33. Academic Press, New York, pp. 295–361.
- Fleck, N.A., Muller, G.M., Ashby, M.F., Hutchinson, J.W., 1994. Strain gradient plasticity: theory and experiment. *Acta Metall. Mater.* 42, 475–487.
- Gao, H., Huang, Y., Nix, W.D., 1999a. Modeling plasticity at the micrometer scale. *Naturwissenschaften* 86, 507–515.
- Gao, H., Huang, Y., Nix, W.D., Hutchinson, J.W., 1999b. Mechanism based strain gradient plasticity I. Theory. *J. Mech. Phys. Solids* 47, 1239–1263.
- George, E.P., Liu, C.T., 2000. Micro- and macro-alloying of Ir-based alloys. In: Iridium, E.K., Ohriner, R.D., Lanam, P., Panfilov and Harada, H. (Eds.). *The Minerals, Metals and Materials Society*, Warrendale, PA, pp. 3–14.
- Huang, Y., Gao, H., Nix, W.D., Hutchinson, J.W., 2000. Mechanism based strain gradient plasticity II. Analysis. *J. Mech. Phys. Solids* 48, 99–128.
- Johnson, K.L., 1970. The correlation of indentation experiments. *J. Mech. Phys. Solids* 18, 115–126.
- Lim, Y.Y., Chaudhri, M.M., 1999. The effect of the indenter load on the nanohardness of ductile metals: an experimental study on polycrystalline work-hardened and annealed oxygen-free copper. *Philos. Mag. A* 79, 2879–3000.
- Lim, Y.Y., Bushby, A.J., Chaudhri, M.M., 1998. Nano and macro indentation studies of polycrystalline copper using spherical indenters. *Mater. Res. Soc. Symp. Proc.* 522, 145–150.
- Liu, C.T., Inouye, H., Schaffhauser, A.C., 1981. Effect of thorium additions on metallurgical and mechanical properties on Ir-0.3 pct W alloys. *Met. Trans. A* 12A, 993–1002.
- Liu, Y., Ngan, A.H.W., 2001. Depth dependence of hardness in copper single crystals measured by nanoindentation. *Scripta Mater.* 44, 237–241.
- Ma, Q., Clark, D.R., 1995. Size dependent hardness in silver single crystals. *J. Mater. Res.* 10, 853–863.
- McElhaney, K.W., Vlassak, J.J., Nix, W.D., 1998. Determination of indenter tip geometry and indentation contact area for depth-sensing indentation experiments. *J. Mater. Res.* 13, 1300–1306.
- Mott, B.W., 1956. *Micro-indentation Hardness Testing*. Butterworths, London.
- Nix, W.D., Gao, H., 1998. Indentation size effects in crystalline materials: a law for strain gradient plasticity. *J. Mech. Phys. Solids* 46, 411–425.
- Nye, J.F., 1953. Some geometric relations in dislocated crystals. *Acta Metall.* 1, 153–162.
- Oliver, W.C., Pharr, G.M., 1992. An improved technique for determining hardness and elastic modulus using load and displacement sensing indentation. *J. Mater. Res.* 7, 1564–1583.
- Poole, W.J., Ashby, M.F., Fleck, N.A., 1996. Micro-hardness tests on annealed and work-hardened copper polycrystals. *Scripta Mater.* 34, 559–564.

- Schultz, F., Hanemann, H., 1941. Die Bestimmung der Mikrohärtigkeit von Metallen. *Z. Metallkd.* 33, 124–134.
- Shaw, C., Li, Y., Jones, H., 1996. Effect of load and lubrication on low load hardness of a rapidly solidified light alloy. *Mater. Ltr.* 28, 33–36.
- Shi, H., Atkinson, M., 1990. A frictional effect in low-load hardness testing of copper and aluminum. *J. Mater. Sci.* 25, 2111–2114.
- Stelmashenko, N.A., Walls, M.G., Brown, L.M., Milman, Y.V., 1993. Microindentation on W and Mo oriented single crystals: an STM study. *Acta Metall. Mater.* 41, 2855–2865.
- Stölken, J.S., Evans, A.G., 1998. A microbend test method for measuring the plasticity length scale. *Acta Mater.* 46, 5109–5115.
- Swadener, J.G., Pharr, G.M., 2000. A methodology for the calibration of spherical indenters. *Mater. Res. Soc. Symp. Proc.* 594, 525–530.
- Swadener, J.G., George, E.P., Pharr, G.M., 2001. A spherical indentation method to determine material length scales, submitted for publication.
- Tabor, D., 1951. *The Hardness of Metals*. Clarendon Press, Oxford.
- Taylor, G.I., 1938. Plastic strain in metals. *J. Inst. Met.* 13, 307–324.
- Wiedersich, H., 1964. Hardening mechanisms and the theory of deformation. *J. Met.* 16, 425–430.